ChemCatChem

Research Article
doi.org/10.1002/cctc.202401863

Chemistry Europe
European Chemical Societies Publishing

www.chemcatchem.org

Cyclopentadienyl Half-Sandwich Rhodium(III) Azopyridine Anticancer Complexes with Activity Tuned by Ligand Substituents

Edward C. Lant,[a] Russell J. Needham,[a] Zijin Zhang,[a, b] James P. C. Coverdale,[a, d] Guy J. Clarkson,[a] Ian Bagley,[c] Robert Dallmann,[b] and Peter J. Sadler*[a]

We report the synthesis and characterization of ten novel half-sandwich Rh(III) azopyridine complexes as potential anticancer agents, with the general formula [(η^5-Cp^x)Rh(4-R$_2$-phenylazopy-5-R$_1$)Cl]PF$_6$, where Cp^x = Cp*, Cp^{xPh} or Cp^{xPhPh}, R$_1$ = H, Br, or CF$_3$, and R$_2$ = H, OH or NMe$_2$. X-ray crystallographic data for complex **2** (R$_1$ = Br, R$_2$ = OH, Cp^x = Cp^{xPh}) and complex **3** (R$_1$ = CF$_3$, R$_2$ = OH, Cp^x = Cp^{xPh}) confirm their typical half-sandwich "piano-stool" geometry. The substituents have a major influence on the cytotoxicity of these complexes toward human ovarian (A2780 and cisplatin-resistant A2780cis), lung (A549) and prostate (PC-3) cancer cells, and non-cancerous human lung fibroblasts (MRC-5). Potencies range from sub-micromolar to inactive (>50 μM). They were non-cross-resistant with cisplatin, and complex **9** (R$_1$ = H, R$_2$ = NMe$_2$, Cp^x = Cp*) showed some selectivity (>3x) for A549 cancer cells versus normal cells. The highly active, lipophilic complex **2** was strongly accumulated by cells and catalyzed the oxidation of NADH (reduced nicotinamide adenine dinucleotide) to NAD$^+$, and GSH (glutathione) to GSSG. Notably, complex **2** is almost an order of magnitude less toxic toward zebrafish in vivo than cisplatin, despite being 10-fold more active in A549 cells. These studies demonstrate how the chemical and biological activities of this series of half-sandwich organorhodium(III) complexes can be finely tuned by the choice of substituents on the cyclopentadienyl and azopyridine ligands. The complexes appear to have an unusual mechanism of anticancer activity, associated not only with Rh(III) but also with the phenylazopyridine, cyclopentadienyl, and the chlorido ligands.

1. Introduction

The success of platinum drugs, cisplatin and its analogues (carboplatin and oxaliplatin), has led to a search for the next generation of transition metal-based anticancer agents, with the goal of reducing doses and side effects, and combatting resistance by introducing new mechanisms of action.[1–4] Recent studies have highlighted the design and application of organometallic metal complexes that can catalyze reactions in biological systems, and offer new avenues for targeted therapy.[5,6] Examples include cyclometalated phenylpyridine Os(II) half-sandwich anticancer complexes, which promote rapid hydrolysis and activation,[7] and metal carbene complexes for in-cell catalysis and synthesis.[8,9] Transfer hydrogenation catalysis in cells is an emerging approach, involving the modulation of cellular redox potentials via the NAD$^+$/NADH couple by Ru(II) catalysts,[10] or the stereospecific reduction of pyruvate by Os(II) catalysts.[11] These studies collectively underline the dual role of organometallic complexes in catalysis and therapeutic intervention, demonstrating their growing importance in innovative cancer treatments and other biomedical applications. Organorhodium compounds have shown promising cytotoxic and potential anticancer properties.[12–24] It is important to investigate the dependence of their chemical and biological reactivity on the oxidation state of the metal, its coordination geometry, and the types and number of ligands, including ligand substituents. Fine-tuning the electronic and steric properties of the bound ligands, and/or varying the metal and its oxidation state, are important for drug design and the construction of structure-activity relationships. For example, changing Ru(II) to Rh(III) in the candidate anticancer drug RAPTA-C [Ru(η^6-*p*-cymene)(pta)Cl$_2$]), (where pta = 1,3,5-triaza-7-phosphatricyclo[3.3.1.1]decane), results in similar cytotoxicity toward A549 lung cancer cells.[23] When co-administrated with a non-toxic dose of sodium formate as a source of reducing hydride, Rh(III) complexes of the general structure [(Cp^x)Rh(N^N)Cl]$^+$ (Cp^x = Cp* or Cp^{xPh},

[a] E. C. Lant, R. J. Needham, Z. Zhang, J. P. C. Coverdale, G. J. Clarkson, P. J. Sadler
Department of Chemistry, University of Warwick, Coventry CV4 7AL, UK
E-mail: p.j.sadler@warwick.ac.uk

[b] Z. Zhang, R. Dallmann
Biomedical Sciences, Warwick Medical School, University of Warwick, Coventry CV4 7AL, UK

[c] I. Bagley
Biomedical Service Unit Research Technology Platform (BSU RTP), Biomedical Sciences, University of Warwick, Coventry CV4 7AL, UK

[d] J. P. C. Coverdale
School of Pharmacy, School of Health Sciences, College of Medicine and Health, University of Birmingham, Edgbaston B15 2TT, UK

Supporting information for this article is available on the WWW under https://doi.org/10.1002/cctc.202401863

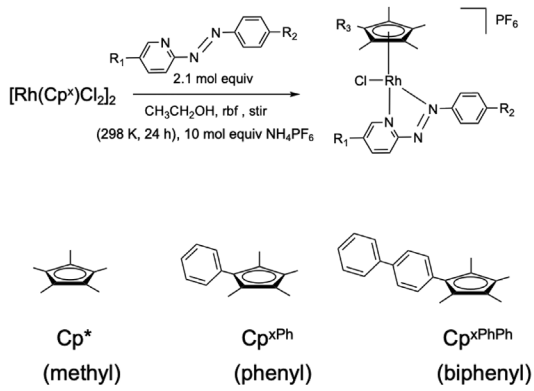

Complex	R_1	R_2	R_3
1	H	OH	Ph
2	Br	OH	Ph
3	CF_3	OH	Ph
4	F	H	Ph
5	H	OH	CH_3
6	H	OH	PhPh
7	Br	H	CH_3
8	Br	H	Ph
9	H	NMe_2	CH_3
10	H	NMe_2	Ph

Scheme 1. Rh(III) azopyridine complexes [(η^5-Cp^x)Rh(4-R_2-phenylazopy-5-R_1)Cl]PF_6 (**1**–**10**) studied in this work and their synthetic route.

N^N = ethylenediamine, 2,2′-bipyridine, 2,2′-dimethylbipyridine, or 1,10-phenanthroline) can catalyze the reduction of intracellular biomolecules such as NAD^+ via a transfer hydrogenation mechanism.[25–28]

The methyl substituents of the Cp^x ring in $[(Cp^x)Rh(N^N)Cl]^+$ complexes (N^N = e.g. bipyridine) have unusual properties.[29] They can be activated by intramolecular proton abstraction by a Rh(III)—OH group following Rh(III)—Cl hydrolysis and undergo rapid H/D exchange, involving Rh(I) fulvene intermediates. These intermediates can be trapped by the formation of Diels–Alder adducts with conjugated dienes, including biologically important dienes, so providing novel reaction pathways for half-sandwich Rh(III) complexes.[30,31] Here, ten novel half-sandwich organorhodium(III) chlorido complexes **1**–**10** (Scheme 1) bearing various substituted bidentate azopyridine ligands have been synthesized, and characterized by ^{1}H and ^{13}C NMR spectroscopy, high-resolution mass spectrometry (HRMS), and HPLC. Their chemical and anticancer properties have been investigated, including the catalytic oxidation of the intracellular coenzyme NADH and abundant tripeptide GSH (γ-L-Glu-L-Cys-Gly). The substituents on the Cp and azpy ligands are shown to have dramatic effects on their activities.

2. Results and Discussion

2.1. Synthesis and Characterization of Complexes

Complexes **1**–**10** were synthesized by reactions of the azopyridine ligands with the appropriate chlorido-bridged dimer (Scheme 1) in good yields of >78%, with an HPLC purity of >97% (see S1.2). NMR and HRMS data were consistent with the proposed structures (see S1.2, Figures S1 and S2). Single crystals suitable for X-ray diffraction of complexes **2·Et$_2$O** and **3·Et$_2$O**, as PF_6^- salts, were obtained at ambient temperature by slow diffusion of Et_2O into saturated dichloromethane solutions (Figure 1 and X-ray crystallographic data listed in Table S8, and selected bond lengths and bond angles in Table S9). The complexes adopt a typical pseudo-octahedral "piano-stool" geometry. Rh-Cl bond lengths (2.3745(14) and 2.3763(10) Å for **2·Et$_2$O** and **3·Et$_2$O**, respectively) and Rh-Cp^x centroid distances (1.495 and 1.500 Å) and related N^N chelated Rh-Cp^{xPh} distances are close to those in similar diamine complexes.[29,32] The N=N azo bonds are slightly lengthened (1.275–1.277 Å) compared to the uncoordinated ligand (1.25 Å).[29,32]

2.2. Hydrolysis

Hydrolysis is a common activation mechanism for chlorido transition metal anticancer complexes, for example, for cisplatin Pt(II)—OH_2 bonds are more reactive than Pt(II)—Cl bonds.[17] The differences in ligand lability across various metal ions are reflected in their aqua ligand exchange rates. Appropriate choices of ligands can modulate hydrolysis activity.[17]

Aquation of chlorido complexes **1**–**10** in 20% MeOD-d_4 / 80% D_2O (1 mM, 310 K) was studied by ^{1}H NMR with peak assignments assisted by comparison of spectra before and after removal of the chlorido ligand by reaction with 1 mol equiv of $AgNO_3$. After 24 h there was ca. 63% hydrolysis for **1,** which was readily reversed by the addition of 2 mol equiv of NaCl (Figures S3–S5). After 24 h, complexes **1**–**6** and **9**–**10** all reached equilibrium for hydrolysis (Table 1). Complexes **7** and **8** were not soluble to 1 mM in MeOD-d_4 for this ^{1}H NMR study. ^{1}H NMR spectra acquired after 24 h incubation at 310 K showed the presence of both the starting complex containing the chelated ligand (4-R_2-phenylazopyridine-5-R_1) and the corresponding aqua complex.

The extent of hydrolysis over 24 h for complexes varied between 0%–100% at equilibrium, based on ^{1}H NMR integrations, as shown for **1** in Figures S3–S5. No apparent hydrolysis was observed for a 1 mM solution of complex **10**, however, hydrolysis was observed at the lower concentrations (20 μM) by UV–vis spectroscopy at 310 K (Figure S7). The pK_a values of the coordinated water in the aqua adduct or phenolic groups on the azpy ligands in these complexes were not investigated in this study. If the pK_a values for the aqua species are <7, then this is likely to result in the formation of hydroxido species at physiological pH (7.4), which might be prone to the formation of bridged species at higher concentrations. The pK_a values for the Ph—OH fragment are likely to lie close to the range 3.90–6.49, based on published data for related Ir(III) Cp^x azpy complexes.[32] These deprotonations might have an effect on the hydrolysis equilib-

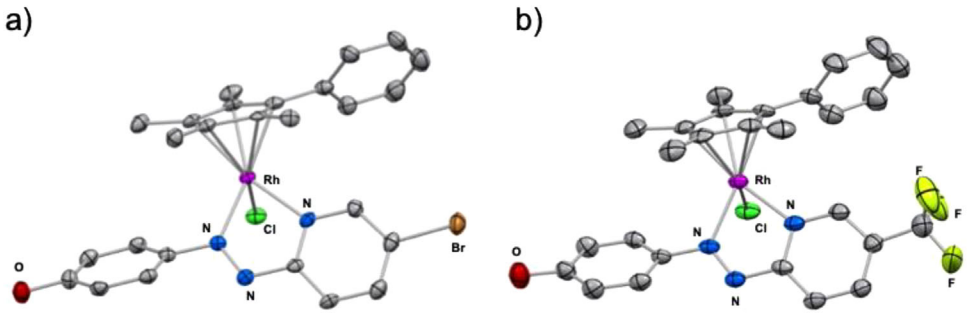

Figure 1. X-ray crystal structures of complexes (a) [(η^5-Cp*)Rh(HO-azpy-Br)Cl]PF_6 (**2·Et$_2$O**) and (b) [(η^5-Cp*)Rh(HO-azpy-CF_3)Cl]PF_6 (**3·Et$_2$O**), with thermal ellipsoids drawn at 50% probability. The hydrogen atoms, counter anions, and solvent molecules are omitted for clarity.

Table 1. Hydrolysis of complexes **1**–**10** studied by ^{1}H NMR in 20% MeOD-d_4/80% D_2O (1 mM, 310 K) and UV–vis spectroscopy in 10% MeOH/90% H_2O (310 K).

Complex	Ligand	Cp^x	Extent (%)[a]	k[b] (min^{-1})	$t_{1/2}$ (min)
1	HO-azpy	Cp^{xPh}	63	0.0038 ± 0.0002	182
2	HO-azpy-Br	Cp^{xPh}	50	0.0030 ± 0.0001	224
3	HO-azpy-CF_3	Cp^{xPh}	73	0.0088 ± 0.0001	78.6
4	azpy-F	Cp^{xPh}	100	0.0062 ± 0.0002	111
5	HO-azpy	Cp*	100	0.0034 ± 0.0001	203
6	HO-azpy	Cp^{xPhPh}	100	0.015 ± 0.003	46,2
7	azpy-Br	Cp*	–	0.015 ± 0.001	46.2
8	azpy-Br	Cp^{xPh}	–	0.012 ± 0.002	57.7
9	Me_2N-azpy	Cp*	100	0.051 ± 0.001	13.6
10	Me_2N-azpy	Cp^{xPh}	0	0.032 ± 0.001	21.7

[a] Determined by ^{1}H NMR peak integrals of the aqua adduct at equilibrium for 1 mM solutions in 20% MeOD-d_4/80% D_2O after 24 h at 310 K;
[b] Apparent pseudo-first-order rate constant determined by fitting the UV–vis absorption changes versus time for 20 μM solutions of the complex in 10% MeOH/90% H_2O (310 K). UV–vis data are shown in Figure S6 for **2** and **9**.

ria, and the species present at pH 7 under biological screening conditions.

Changes in the UV–vis spectra were monitored for 20 μM solutions of the complexes in MeOH/H_2O v/v. Half-lives varied between ca. 14 and 224 min for complexes **9** and **2**, respectively. Complex **9** has the electron-donating NMe_2 substituent on the azopyridine and a Cp*, whilst **2** has an electron-withdrawing Br group on the pyridine and a phenyl group on the Cp^x ring.

2.3. Electrochemical Reduction

Electrochemical reduction of complexes **2** and **9** in methanol was studied by cyclic voltammetry (CV) under N_2 versus a Ag^+/Ag reference electrode. For both complexes, the first reduction step was quasi-reversible (−0.586 and −0.795 V for **2** and **9**, respectively), but the second was weak and irreversible Table S1 and Figure S8. The first reduction potential becomes more positive as the Cp^x ring is extended from Cp* to Cp^{xPh} and as the chelating azo ligand is changed from Me_2N-azpy, to HO-azpy-Br. This reduction potential can be assigned to the addition of an electron into the π^* orbital centered on the azo group of the azopyridine ligands to form the azo anion radical (—N=N— + e^- → {—N—N—}$^-$).[33] The relative order therefore reflects the decreasing π-acceptor capability of the substituted azpy ligands with the addition of electron-donating groups onto the phenyl ring.[33,34] The irreversible second reduction step is assigned to conversion to the dianionic species ({—N—N—}$_2^-$). Azo groups usually give rise to two separate electrochemical reductions in polar aprotic solvents.[33,34] In aqueous media, the two-electron reduction of azo groups is accompanied by proton transfer to give hydrazo groups (NH—NH) in a single step.[33,34]

In comparison with reported electrochemical data on related half-sandwich azpy complexes (Table S2), the first reduction potentials for the Ru(II) complex [(η^6-pcym)Ru(Me_2N-azpy)I]$^+$ (**Ru-a**)[35] and Os(II) complex [(η^6-pcym)Os(Me_2N-azpy)I]$^+$ (**Os-b**)[36] are higher than for the Rh(III) complex [(η^5-Cp*)Rh(Me_2N-azpy)Cl]$^+$ (**9**): **9** (MeOH) < **Os-b** (CH_3CN) < **Ru-a** (DMF). Although the solvents used are different, they have similar dielectric constants (33–37).[37] Since the complexes all have the same azpy ligand, the data illustrate that the metal ion, arene/Cp^x, and monodentate (Cl/I) ligands can all modulate the overall redox properties of the complexes. The first reduction potentials are lower than the biologically relevant range, for example, for GSH/GSSG −240 mV at pH 7,[38] noting that the latter value is for an aqueous medium in comparison to MeOH used here.

Table 2. IC_{50} values for complexes **1–10** and cisplatin (CDDP) in human A549 lung, PC-3 prostate, A2780 ovarian, and A2780cis cisplatin-resistant ovarian cancer cells, and normal MRC-5 fetal lung fibroblasts. Growth inhibition curves are shown in Figures S14–S21.

Complex	A549 IC_{50} /(μM)[a] (RF)[b]	PC-3	A2780	A2780cis	MRC-5
1	3.7 ± 0.1	6 ± 1	–	–	–
2	0.8 ± 0.1	1.4 ± 0.1	1.4± 0.1	0.35 ± 0.03 (0.2)	1.4 ± 0.4
3	1.5 ± 0.2	2.9 ± 0.4	4.5 ± 0.1	0.8 ± 0.2 (0.2)	1.6 ± 0.1
4[c]	>50	>50	–	–	–
5[c]	>50	>50	–	–	–
6	5.5 ± 1.3	4.0 ± 0.9	–	–	–
7	33 ± 12	19.6 ± 0.8	–	–	–
8	13 ± 1	11.9 ± 0.2	–	–	–
9	29.9 ± 0.5	18 ± 4	8 ± 0.5	7 ± 1 (0.9)	>100
10	6 ± 2	12 ± 2	–	–	–
CDDP	6.6 ± 0.1	1.7 ± 0.4	1.4 ± 0.1	12.2 ± 0.2 (8.8)	7.6 ± 0.6

[a] IC_{50} values are the mean ± standard deviations for two independent experiments, each carried out in triplicate. Cancer cells were exposed to the test complex for 24 h followed by 72 h recovery time in fresh medium.
[b] Resistance factor RF = IC_{50}(A2780cis)/IC_{50}(A2780).
[c] 100 μM highest test dose, see Figures S14d and S15e.

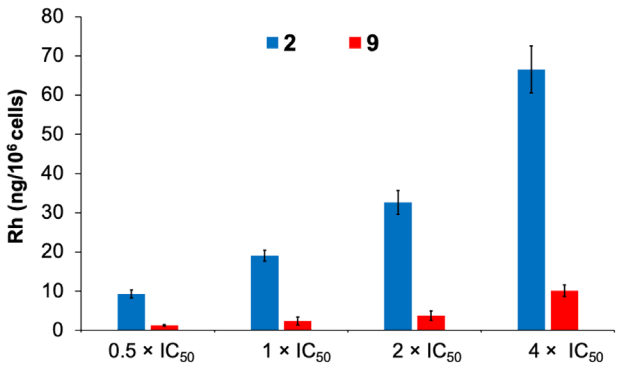

Figure 2. Accumulation of Rh (ng/10^6 cells) in A549 human lung cancer cells after 24 h treatment with complex **2** or **9** at concentrations of 0.5x IC_{50}, 1x IC_{50}, 2x IC_{50}, and 4x IC_{50}. The values represent mean ± standard deviations for three independent biological replicates ($N = 3$).

2.4. Antiproliferative Activity (IC_{50})

Since for biological studies the rhodium complexes were prepared in 5% DMSO, 95% DMEM, v/v, to aid solubility, the stability of complexes **1–10** in DMSO for 24 h was studied by ^{1}H NMR (400 MHz, DMSO-d_6). No spectral changes were observed indicative of their high stability in this solvent.

The antiproliferative activities of complexes **1–10** and cisplatin were determined toward human lung A549 (Table 2), and prostate PC-3 cancer cell lines using the SRB assay[39] (Table 2). Some of these complexes display potent cytotoxicity, with IC_{50} values in the range of 0.2 to 29.9 μM (Table 2). The order of potency in A549 cells was: **2** (most potent) > **3** > **1**, **CDDP**, **6**, **10** > **8** > **9**, **7** > **4**, and **5** (least potent).

Complex **2** [(Cp^{xPh})Rh(HO-azpy-Br)Cl]PF_6 was 10-fold more active than cisplatin. In contrast, complexes **7** [(Cp^{xPh})Rh(azpy-Br)Cl]PF_6 and **9** [(Cp*)Rh(Me_2N-azpy)Cl]PF_6 were less active. Interestingly, complexes **4** and **5** both showed poor activity (IC_{50} > 50 μM). The most active complexes (**2**, **3**, and **1**) all contain an extended Cp^{xPh} ring and a hydroxyl substituent on the phenyl group of the azpy ligand. Under physiological conditions, it is likely that the OH group is deprotonated (pK_a <7), as is the case for the analogous Ir(III) complexes,[32] hence the chlorido complexes would be neutral, enhancing cellular uptake. They would also be zwitterions. Guo et al. have reported potent activity for zwitterionic Rh(III) half-sandwich sulfonated iminopyridine complexes, which initially target lysosomes.[40]

A similar order of potency was observed for PC-3 prostate cancer cells (Table 2): **2** (most potent), CDDP, **3**, **6**, **1** > **8**, **10** > **9**, **7** > **4**, and **5** (least potent).

The relative potency toward the normal lung cell line MRC-5 for complexes **2** and **3** versus the cancer cell line A549, indicates a poor selectivity, perhaps influenced by their lipophilicities and cell uptake. Complex **9** showed promising selectivity of >3 for cancer cells over non-cancerous cells: IC_{50} 29.9 ± 0.5 μM in A549 lung cancer cells, compared to >100 μM in MRC-5 lung fibroblast cells.

The accuracy by which some of the IC_{50} values could be determined was limited by the shapes of some of the dose-response sigmoidal plots, Figures S14–S21. Notably, the highly active complexes 1, 2, and 6, exhibited an abrupt decrease in cell viability as the administered dose was increased (Figures S15 A549, S17, S18 PC-3, S20 A2780 and S21 MRC-5). This sharp, rapid decrease in cell percentage viability relative to the untreated control may be correlated with the mechanism of cell death and suggests possible necrosis, involving a sudden disintegration of the plasma membrane.[41,42] Further investigation of plasma membrane targeting is underway, but beyond the scope of the present study.

Based on their high in vitro activity, complexes **2** and **3,** along with complex **9**, were selected for further screening against human ovarian cancer cells (A2780) and cisplatin-resistant A2780 ovarian cancer cells (A2780cis) to examine cross-resistance with cisplatin (Table 2). Complexes **2** and **3** were ca. 60× and

15× more potent than cisplatin toward the drug-resistant cell line, while complexes **2**,**3**, and **9** were not cross-resistant with cisplatin, with resistance factors IC_{50}(A2780cis)/IC_{50}(A2780) of 0.3, 0.7, and 0.9, respectively.

It is notable that within a family of reported half-sandwich azpy Ru(II), Os(II), Rh(III), and Ir(III) complexes (Ru-**a**, Os-**a**, Os-**b**, and Ir-**c**, Table S3), the anticancer activity in, for example, A549 lung cancer cells can vary from highly potent nanomolar activity for Ir-**c**,[32] and Rh **2**, which differ only in the I/Cl monodentate ligand), to inactivity (Rh **4**, Ru-**a**).[35] This illustrates the fine-tuning available within this family of half-sandwich complexes as a platform for drug design for consideration of both activity, targeting, and minimizing side effects.

2.5. Cellular Rh Accumulation

To elucidate factors that influence the observed anticancer activities, cellular Rh accumulation was quantified in A549 cells by ICP-MS after 24 h treatment with complexes **2** and **9** at equipotent concentrations of 0.5×,1×, 2×, and 4× IC_{50} at 310 K (Table S4). Rh accumulation increased in a concentration-dependent manner. After 24 h, cellular Rh accumulation in cells treated with equipotent concentrations of more potent complex **2** was ca. eightfold higher than in cells treated with less potent complex **9** (Figure 2). Hence, the extent of drug accumulation may play a major role in the activity.

2.6. Lipophilicity and Anticancer Activity

Capacity factors (*K*) measure the affinity of a compound toward the HPLC stationary phase, and hence provide a measure of the relative lipophilicity of complexes. Capacity factors were determined for complexes **2**, **3**, **9**, and **10** (as examples of complexes with either high or low antiproliferative activity) using an isocratic HPLC method at 298 K, relative to the retention time of uracil, Table S6. The mobile phase was H_2O: MeOH (1:1, v/v) containing 50 mM NaCl, and the stationary phase was a reverse-phase C18 column (250 × 4.6 mm column with a pore size of 5 μm). Correlations between antiproliferative activity toward A549 cells and capacity factor are shown in Figure 3.

A strong inverse correlation is observed (−0.92, Figure 3); that is, when the relative lipophilicity increases, the IC_{50} value decreases (increased activity), which is overall likely due to the improved cellular accumulation of complexes exhibiting higher lipophilicity. Complex **2** showed the highest capacity factor and hence was the most lipophilic complex. The trend for increasing lipophilicity is **9** <**10** <**3** <**2**, that is, increasing with extension to the substituent on the Cp^x ring (i.e., Cp^{xPh} >Cp*). This is clearly demonstrated by complexes **9** and **10,** both of which contain the same azpy ligand substituents.

2.7. ROS Studies

Levels of reactive oxygen species (ROS) and superoxide (SO) were quantified in A549 human lung cancer cells treated with complex **2** or **9** using flow cytometry (Figure 4). Superoxide production was monitored in the orange channel FL1, and total ROS species (including H_2O_2, peroxy and hydroxyl radicals, and peroxynitrite and NO) were monitored by the green channel FL2. After 24 h exposure, an increase in ROS levels was observed in cells treated with **2** or **9**, relative to the untreated (stained) negative control. Elevated levels of superoxide were also observed in cells treated with complex **2** but not **9**. Similarly, superoxide (SO) generation has been reported for related cytotoxic azpy complexes of Os(II), Ru(II), and Ir(III).[32,35,43] The observation of the burst of SO generation observed in the Ir(III) azpy analogues[32] strongly points toward the importance of the azpy ligands in the production of these species.

2.8. In Vivo Activity

Since the compounds showed promise as anticancer therapeutics in vitro, in vivo toxicities were investigated using zebra fish embryos. The zebra fish model has been shown to closely model toxicity in humans.[44,45] LD_{50} concentrations were determined following the well-established zebra fish embryo toxicity test (Figure 5). Strikingly, rhodium complexes **2** and **9** (LD_{50} = 4.8 ± 0.2 μM and 1.1 ± 0.1 μM, respectively) were up to eightfold less toxic toward zebra fish embryos than cisplatin (LD_{50} = 0.6 ± 0.2 μM in SG-WT). The second-generation platinum anticancer drug, carboplatin, was an order of magnitude less toxic than cisplatin (LD_{50} = 5.7 ± 0.9 μM in SG-WT) toward zebra fish.[43]

Whole-mount zebra fish embryos were exposed to equipotent solutions of Rh(III) complexes **2** and **9** (1.0 × IC_{50}) for 96 h and anesthetized. Levels of reactive oxygen species were determined using a green fluorescent probe to detect ROS (including H_2O_2, peroxynitrite, and hydroxyl radicals) and analyzed using confocal microscopy. Embryos were stained using the reagent of the ROS/Superoxide Detection Assay (Enzo Life Sciences) for ROS detection with excitation at 458, 488, and 561 nm and green emission for ROS at 493–550 nm.[46] Pyocyanin was used as a positive control. Dye localization was observed in the positive control, (Figure 5c, zebra fish embryos exposed to 50 μM of pyocyanin for 5 min).

In general, high intracellular ROS generation causes cell death by activating cell death pathways (both mitochondrial-dependent and independent).[47–49] However, low levels of ROS act as signaling molecules that facilitate cell survival.[47–49] There are distinct differences in the extent and localization of the signal attributed to the production of ROS in embryos treated with **2** and **9**. Embryos incubated with **2** exhibited fluorescence localized in a region of the rhombencephalon or hindbrain (hb) (Figure 5b), whereas embryos treated with **9** displayed a much greater concentration of ROS fluorescence extending from the yolk sac (ys) to the caudal vein (cv) (Figure 5d). The differences in ROS signals between **2** and **9** correlate with the in vitro ROS induction study (Table 2 and Figure 4) whereby **9** induces greater ROS levels in comparison to **2**, which may be related to the efficiency of radical generation.

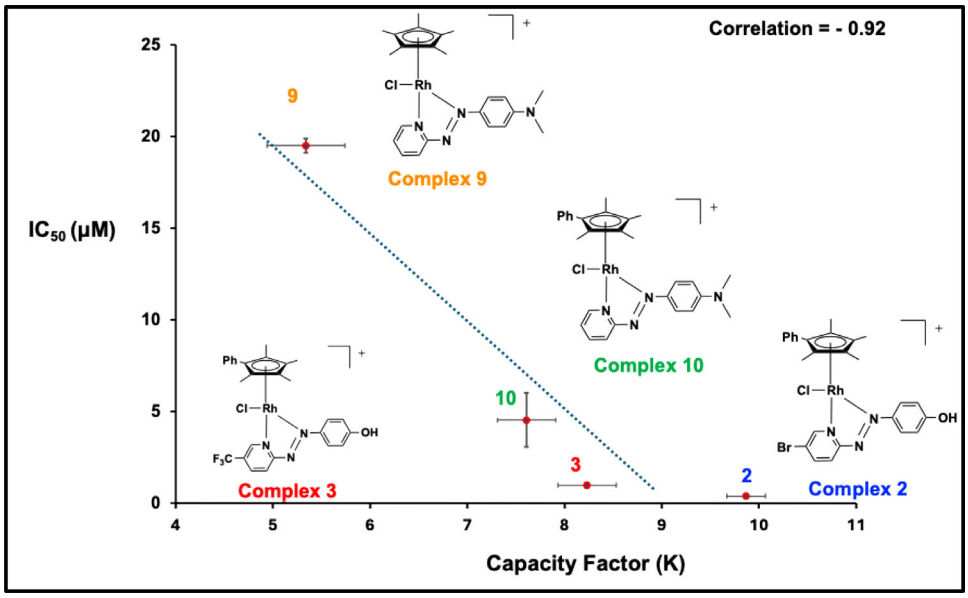

Figure 3. Plot of antiproliferative activity (IC_{50} toward A549 cells, μM) versus capacity factor (*K*), for complexes **2**, **3**, **9**, and **10** in which substituents on the azpy and Cp^x ligands are varied. In general, the most lipophilic complexes are the most active. Highly active complex **2** is likely to have a deprotonated phenoxide group at pH 7.4. It has a higher lipophilicity (capacity factor, Table S6) and cell uptake (Figure 3) than complex **9**.

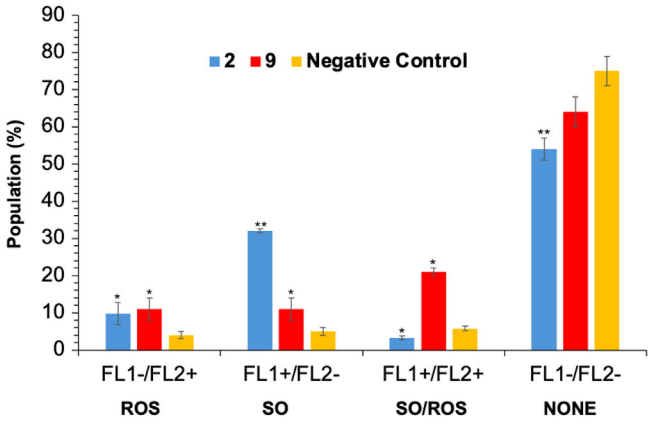

Figure 4. Cell population for total ROS and superoxide production in A549 cancer cells exposed to complex **2** or **9** at IC_{50} concentrations of **2** (0.5 μM) and **9** (29.9 μM) for 24 h with untreated cells as the negative control. FL1 channel detects superoxide production, and FL2 channel detects total oxidative stress. Normalized population data are presented as the mean ± SD of triplicate samples for one experiment. p-Values were calculated after a t-test against the negative control data, $*p < 0.05$, $**p < 0.01$. See Table S5 for full numerical data.

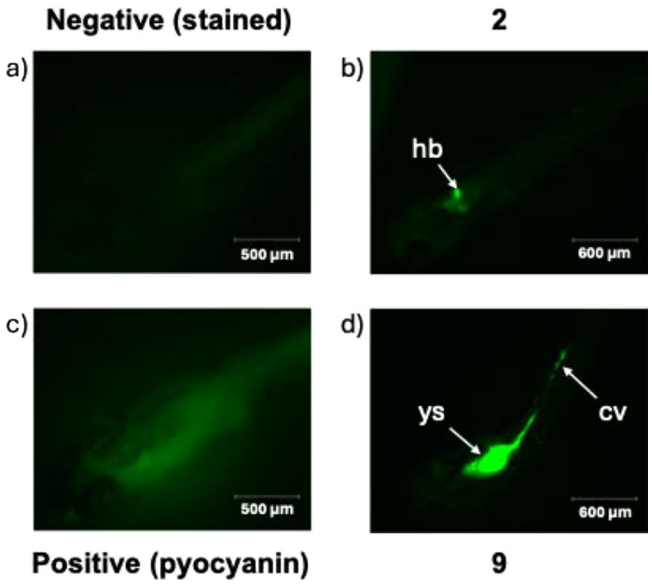

Figure 5. Fluorescence imaging of ROS (green) for whole-mount SG-WT zebra fish (*Danio rerio*) treated with Rh(III) complexes (1.0 × IC_{50}) (b) **2** and (d) **9** for 96 h. (b) Embryos incubated with **2** exhibited fluorescence localized in the hindbrain (hb). (d) Whereas embryos treated with **9** displayed fluorescence extending from the yolk sac (ys) to the caudal vein (cv). Confocal images were acquired using a Zeiss LSM880 confocal microscope. Embryos were stained using the reagent of the ROS/Superoxide Detection Assay (Enzo Life Sciences) for ROS detection. Excitation at 458 and 488 nm; green emission for ROS at 493–550 nm.[46] Pyocyanin was used as a positive control; the negative control was stained using 2 μM of ROS detection reagent.

2.9. Catalytic Oxidation of NADH

The cofactor 1,4-NADH is an important hydride source in cells.[10,50,51] Its oxidation to NAD^+ by Rh(III) complexes **2** and **9** was monitored using UV–visible spectroscopy for 24 h at 298 K, with 25, 50, and 100 μM 1,4-NADH (Figure 6). Conversion was determined by measuring the absorbance at 339 nm, corresponding to 1,4-NADH (Figure 6). Turnover numbers (moles of NADH converted per mol of catalyst in 24 h) and maximum turnover frequencies (TOF_{max}/h^{-1}) were then calculated (Figure 7 and Table 3). Both complexes catalyze the oxidation of 1,4-NADH to NAD^+. The initial rate was greater for catalyst **9** for all three concentrations of 1,4-NADH (TOF_{max} = 4.93 h^{-1} for 100 mol equiv.) compared to catalyst **2** (TOF = 1.43 h^{-1}). This may be related to the faster rate of hydrolysis of complex **9** compared to complex **2** and the higher reactivity of the aqua species. In the presence of 25 or 50 μM NADH, complex **9** (bearing a Cp* unit) showed a respective ca. twofold or ca. fourfold higher TOF_{max} than Cp^{xPh} complex **2**. This is similar to previous stud-

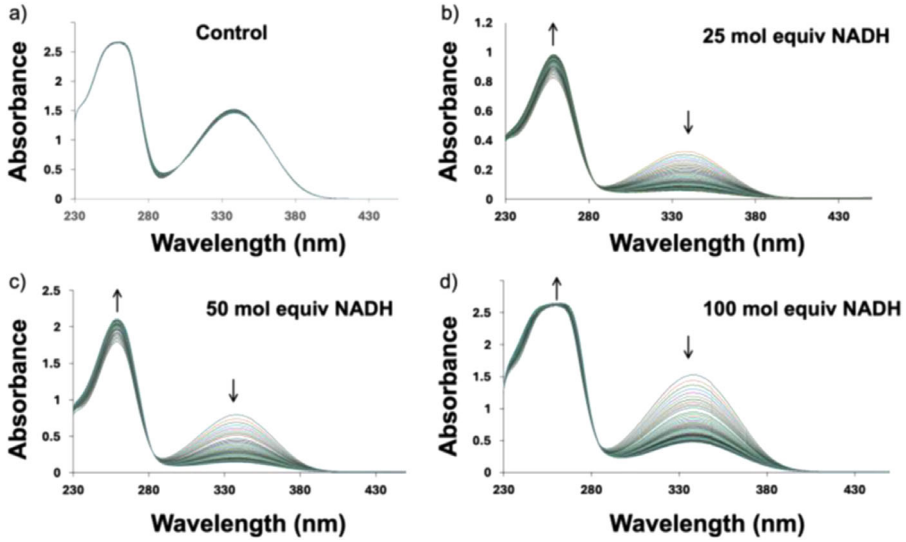

Figure 6. UV–vis absorption spectra recorded every hour for 25, 50, or 100 mol equiv of NADH in the presence of 2 μM complex (a) control (ca. 200 μM NADH) (b) **9** with 25 mol equiv NADH (c) **9** with 50 mol equiv, and (d) **9** with 100 mol equiv after 24 h in 1.6% MeOH/98.4% 5 mM phosphate buffer (pH 7.4) at 310 K. The turnover number (TON) and maximal turnover frequency (TOF_{max}) were determined based on the decrease in absorption of NADH at 339 nm due to the conversion of NADH to NAD^+ over 24 h. In (a) and (d), the intensity of the peak at 252 nm is affected by the limit of detection.

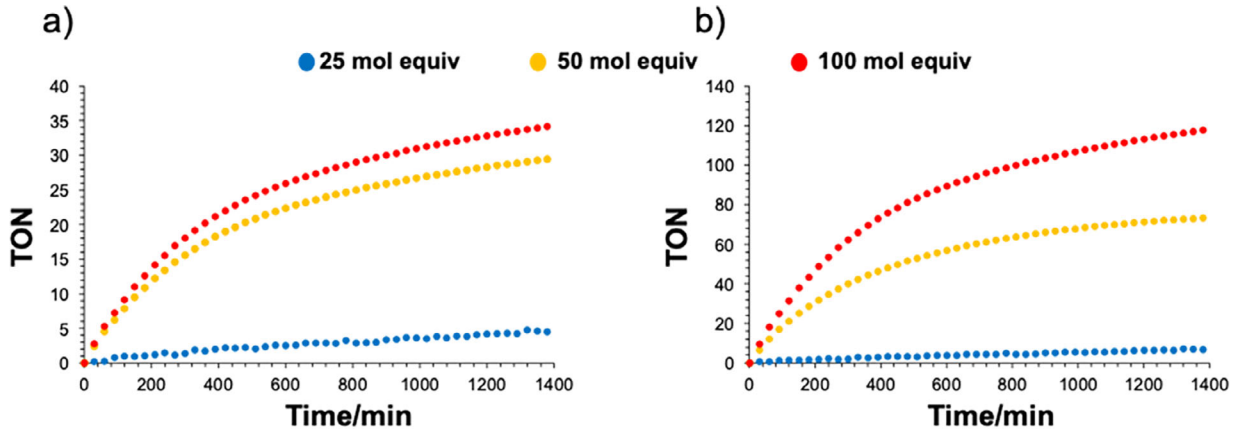

Figure 7. Plots of turnover number versus time for the catalytic oxidation of NADH at three different molar equivalents of NADH (25, 50 or 100 μM) by complexes (a) **9** (2 μM) and (b) **2** (2 μM) in 1.6% MeOH/98.4% v/v, 5 mM phosphate buffer (pH 7.4) at 293 K.

Table 3. TONs and TOFs for oxidation of NADH to NAD^+ by **2** and **9** in 1.6% MeOH/98.4% 5 mM Na_2HPO_4-NaH_2PO_4 buffer (pH 7.4).

Catalyst	NADH (mol equiv)	TON	TOF_{max} (h^{-1})
2	25	2	0.08 ± 0.01
2	50	30	1.23 ± 0.05
2	100	34	1.43 ± 0.06
9	25	8	0.31 ± 0.01
9	50	74	3.06 ± 0.01
9	100	118	4.93 ± 0.02

ies of $[(Cp^x)Rh(diamine)Cl)]^+$ complexes, for which the catalytic activity (TOF) for the reduction of NADH increased in the order en <phen <bpy and the TOF was also lower for extended Cp^{xPh} or Cp^{xPhPh} rings.[51]

These reactions may also be influenced by steric factors caused by the size of the extended Cp^x ring and the chelated ligand. In a related study involving the generation of NADH from NAD^+ using formate as the hydride source and Rh(III) complexes with N^N-substituted 2,2′-bipyridine ligands, the substituents strongly influenced catalytic activity.[51] Hydrogen peroxide was also detected semi-quantitatively (appearance of blue color on Quantofix test sticks) in a reaction mixture of complex **9** (ca. 1 mM) with 3.0 mol equiv. NADH in MeOH/H_2O (1/1 v/v) after 24 h at 310 K (Figure S9) showing ca. 5 mg/L H_2O_2, implicating a role for O_2 in the catalytic cycle.

2.10. Reactions with Glutathione

In cells, a major reducing agent is the intracellular tripeptide glutathione (GSH, γ-L-Glu-L-Cys-Gly), a thiol present at millimolar concentrations which acts as a detoxification agent and ROS scavenger.[52] Reactions of **9** $[(Cp^*)Rh(Me_2N\text{-azpy})Cl]^+$ and **2** $[(Cp^{xPh})Rh(HO\text{-azpy-Br})Cl]^+$ (100 μM) with GSH (10 mM) in phosphate buffer (20 mM, pH 7.4) were monitored over 24 h

by HPLC/LC-MS (Figure S10). From the ESI-MS of the HPLC peaks (Figure S11 and Table S7) ca. 95% of **9** was converted to the glutathione adduct $[(Cp^*)Rh(Me_2N\text{-azpy})(SG)]^+$ (m/z 768.21 $[M + SG]^+$), (**9-SG**) within the first 10 min, and was the major species in solution over 24 h. In contrast, no adduct formation was observed for **2** after 24 h, correlating with its slower rate of hydrolysis (Table 1).

2.11. Catalytic Oxidation of Glutathione

Reactions of complex **2** and **9** (100 μM) with glutathione (10 mM) in phosphate-buffered saline (20 mM, pH* 7.4) at 310 K were also monitored by ^{1}H NMR for 24 h. The formation of oxidized glutathione (GSSG) was evident from the appearance of new resonances at $\delta = 3.30$ ppm, corresponding to the $\beta_{\text{-CH2}}$ of GSSG from the reaction of complex **9** (TON = 27 ± 1, Figure S12). In contrast, no oxidation was observed in the presence of complex **2**. There are reports of azo compounds facilitating the oxidation of GSH, including the Hodgkin's and non-Hodgkin's lymphoma drug procarbazine, a hydrazo compound that is readily oxidized to the corresponding azo compound and re-reduced via GSH oxidation to GSSG.[53] Interestingly, analogous GSH adducts of Ru(II) and Os(II) arene complexes can undergo oxidation at the coordinated sulfur.[54,55] The re-oxidation of this hydrazo group is facilitated by O_2 inside cells, which is hydrogenated to form H_2O_2.[54,55] Future investigations into the role of the azo bond in the catalytic cycle are therefore warranted.

Studies have also shown that the oxidation of GSH to GSSG is not induced by the free azopyridine ligands.[54,55] This is perhaps not surprising because electron-donating groups attached to the azo ligands (in this instance OH or NMe_2) decrease their ability to oxidize GSH.[39] The first step in the electrochemical reduction of azo ligands can be assigned to the one-electron addition into the π^* orbital centered on the azo group to give the azo anion radical.[34,56,57] The second one-electron reduction gives rise to the dianionic species ([—N—N—]$^{-2}$). In aqueous media, two-electron reduction is also accompanied by proton transfer to give hydrazo groups [—NH—NH—].[34] Since the redox potential for GSH/GSSG (−240 mV at pH 7)[34,58,59] is less negative than those of the azpy Rh(III) complexes **2** and **9**, (Table S1) and outside the biologically relevant region of −430 and −273 mV,[38] these complexes are less easily reduced. This suggests that these complexes are less likely to be reduced by GSH than in their Ir(III) analogues.[32] Overall, the catalytic oxidation of GSH to GSSG by Rh(III) complexes is not as efficient as for their Ir(III) analogues, and may point toward a different mechanism of action for this class of Rh(III) Cp^x azopyridine compounds.

3. Conclusions

The synthesis and characterization of novel azopyridine Rh(III) anticancer complexes **1**–**10** has allowed the dependence of their chemical and biological activities on substituents on the Cp ring and chelated azpy ligands to be studied. The complexes have typical "piano-stool" half-sandwich configurations, as exemplified by the X-ray crystal structures of highly cytotoxic complexes **2** and **3**.

This study reveals how significant variations in the cytotoxicity of Rh(III) azopyridine complexes depend on both ligand substituents and cellular interactions. For example, complexes **1**, **5**, and **6** containing the HO-azpy ligand differ only in the extension of the Cp^x ligand, with **1** containing Ph, **5** CH_3, and **6** PhPh as substituents. However, this results in 30x and 1.5x increase in cytotoxicity for **1** and **6**, respectively, compared to **5** in A549 cells. Similarly, for complexes **9** and **10**, which both contain the Me_2N-azpy ligand and again differ only in the extension of the Cp^x ligand, with **10** containing an extended Ph substituent. A similar increase in cytotoxicity is observed, with **10** being slightly more active than **9** in A549 and PC-3 cells (Table 2). Another example shows that in a comparison of the cytotoxicity of **2** with **1**, which differ only in the addition of a Br group on the azpy ligand in **2** and there is a 5x increase in activity in A549 and PC-3 cells.

Importantly, neither complex **2** nor **9** was cross-resistant with cisplatin, suggesting a distinct mechanism of action which may not involve DNA targeting, the classical mechanism for current clinical platinum drugs cisplatin and carboplatin. The sudden onset of cell death apparent in some cell growth inhibition plots (Figures S14–S21) suggests that necrosis may play a role in the mechanism of cell death for some of the complexes studied here, and correlate with the ability of these complexes to target cell membranes.

Despite the ability of **9** to catalyze the oxidation of GSH and NADH, its IC_{50} (29.9 μM in A549) was significantly higher than that of **2**. However, **9** exhibited promising selectivity for cancer cells over non-cancerous cells. In vivo zebra fish toxicity studies revealed that both **2** and **9** were significantly less toxic than cisplatin. ROS generated by complex **2** were localized primarily in the zebra fish hindbrain, whereas ROS generated by **9** were more widespread, extending from the yolk sac to the caudal vein. These results are consistent with ROS induction studies in A549 lung cancer cells. Complex **2** demonstrated eightfold greater rhodium accumulation in A549 cells compared to **9** (Table 2), likely a consequence of its higher relative lipophilicity. Nonetheless, complex **9** exhibited the highest catalytic activity for NADH oxidation. Complex **9** also reacted more rapidly with GSH, which might result in greater cellular deactivation, and thus contribute to the higher potency of **2** compared to **9** in lung cancer cells. However, for the analogous Ir(III) azpy complexes, DFT calculations have suggested that a plausible pathway for the GSSG formation involves the initial formation of the GSH adduct.[32]

The findings in this study illustrate that the rational design of these half-sandwich anticancer complexes as complexes with unusual mechanisms of action can be fine-tuned by the choice of substituents on the azpy and cyclopentadienyl ligands.

4. Experimental Section

4.1. General Procedures

Rhodium chlorido complexes **1**–**10** (Scheme 1) were synthesized by the same general procedure as follows: the ligand (2.1 mol equiv) was added to a 10.0 mL ethanol solution of $[(\eta^5\text{-}Cp^x)Rh(\mu\text{-}Cl)Cl]_2$ (Cp^x = Cp* or Cp^{xPh}, 1.0 mol equiv). The mixture immediately

turned to dark red and was stirred at ambient temperature for 24 h. Substituted azopyridine ligands HO-azpy-Br, HO-azpy-CF_3 and HO-azpy, azpy-Br and azpy-F were synthesized and characterized according to reported procedures as reported in the Supporting Information.[2,3]

4.2. X-Ray Crystallography

X-ray crystallographic data for complexes **2** and **3** have been deposited in the Cambridge Crystallographic Data Centre under the accession numbers CCDC 2390246–2390247, respectively. X-ray crystallographic data in CIF format are available from the Cambridge Crystallographic Data Centre (http://www.ccdc.cam.ac.uk/).

More detailed experimental procedures can be found in the Supporting Information where the authors have cited additional references.

Author Contributions

Edward C. Lant and Peter J. Sadler conceived the project, planned the experiments, and interpreted data. Edward C. Lant and Russell J. Needham designed and synthesized the ligands and complexes, characterized by Edward C. Lant. Guy J. Clarkson carried out the X-ray crystallography. Hydrolysis and redox reactions were carried out by Edward C. Lant. Cytotoxicity screening was carried out by Zijin Zhang, Edward C. Lant and Robert Dallmann, Rh accumulation assays by Zijin Zhang and Edward C. Lant, and zebrafish screening by James P. C. Coverdale, Edward C. Lant, and Ian Bagley. The paper was drafted by Edward C. Lant and Peter J. Sadler and all authors contributed to the final version.

Acknowledgements

We thank the Engineering and Physical Sciences Research Council (EPSRC, grant no. EP/F034210/1 and EP/P030572/1), Anglo American Platinum, China Scholarship Council (Studentship for ZZ), the Royal Society of Chemistry (grant no. E22-1637945680 for JPCC) and Warwick Analytical Science CDT/Bruker (studentship for ECL) for funding. We thank Dr. Lijiang Song for assistance with mass spectrometry, Dr. Ivan Prokes with NMR spectroscopy, and Drs. Oliver Carter and Cinzia Imberti with cell culture and cytotoxicity assays.

Conflict of Interests

The authors declare no conflict of interest.

Data Availability Statement

The data that support the findings of this study are available in the supplementary material of this article.

Keywords: Azopyridine ligands · Cancer cell cytotoxicity · Half-sandwich complexes · Reactions with biomolecules · Rh(III) cyclopentadienyl catalysts

[1] K. Peng, Y. Zheng, W. Xia, Z. W. Mao, *Chem. Soc. Rev.* **2023**, *52*, 2790–2832.
[2] A. M. Florea, D. Büsselberg, *Cancers* **2011**, *3*, 1351–1371.
[3] S. Dasari, P. B. Tchounwou, *Eur. J. Pharmacol.* **2014**, *740*, 364–378.
[4] M. Hanif, C. G. Hartinger, *Future Med. Chem.* **2018**, *10*, 615–617.
[5] S. Alonso-de Castro, A. Terenzi, J. Gurruchaga-Pereda, L. Salassa, *Chem. - Eur. J.* **2019**, *25*, 6651–6660.
[6] A. L. Noffke, A. Habtemariam, A. M. Pizarro, P. J. Sadler, *Chem. Commun.* **2019**, *48*, 5219–5246.
[7] T. C. Chang, K. Tanaka, *Bioorg. Med. Chem.* **2021**, *46*, 116353.
[8] S. Infante-Tadeo, V. Rodríguez-Fanjul, C. C. Vequi-Suplicy, A. M. Pizarro, *Inorg. Chem.* **2022**, *61*, 18970–18978.
[9] S. Gutiérrez, M. Tomás-Gamasa, J. L. Mascareñas, *Chem. Sci.* **2022**, *13*, 6478–6495.
[10] S. Banerjee, P. J. Sadler, *RSC Chem. Biol.* **2021**, *2*, 12–29.
[11] J. P. Coverdale, I. Romero-Canelón, C. Sanchez-Cano, G. J. Clarkson, A. Habtemariam, M. Wills, P. J. Sadler, *Nat. Chem.* **2018**, *10*, 347–354.
[12] Y. B. Peng, W. He, Q. Niu, C. Tao, X. L. Zhong, C. P. Tan, P. Zhao, *Dalton Trans.* **2021**, *50*, 9068–9075.
[13] M. C. Risi, J. Stjärnhage, W. Henderson, J. R. Lane, C. G. Hartinger, G. C. Saunders, *Dalton Trans.* **2025**, *54*, 539–549.
[14] C. H. Leung, H. J. Zhong, D. S. H. Chan, D. L. Ma, *Coord. Chem. Rev.* **2013**, *257*, 1764–1776.
[15] Y. Geldmacher, M. Oleszak, W. S. Sheldrick, *Inorganica Chim. Acta* **2012**, *393*, 84–102.
[16] G. Gasser, I. Ott, N. Metzler-Nolte, *J. Med. Chem.* **2011**, *54*, 3–25.
[17] E. J. Anthony, E. M. Bolitho, H. E. Bridgewater, O. W. Carter, J. M. Donnelly, C. Imberti, E. C. Lant, F. Lermyte, R. J. Needham, M. Palau, P. J. Sadler, *Chem. Sci.* **2020**, *11*, 12888–12917.
[18] C. M. Bernier, C. M. DuChane, J. S. Martinez, J. O. I. I. Falkinham, J. S. Merola, *Organometallics* **2021**, *40*, 1670–1681.
[19] V. S. da Silva, R. M. Dantas, M. José, S. Mesquita, B. A. Rodrigues, S. C. Correia, D. O. da Silva Mendes, A. C. de Melo Cotrim, J. L. da Silva Gonç, W. B. dos Santos, *Adv. Biol. Chem.* **2025**, *15*, 1–7.
[20] P. Štarha, Z. Dvořák, Z. Trávníček, *J. Organomet Chem.* **2018**, *872*, 114–122.
[21] J. Liang, A. Levina, J. Jia, P. Kappen, C. Glover, B. Johannessen, P. A. Lay, *Inorg. Chem.* **2019**, *58*, 4880–4893.
[22] G. J. Yang, W. Wang, S. W. F. Mok, C. Wu, B. Y. K. Law, X. M. Miao, K. J. Wu, H. J. Zhong, C. Y. Wong, V. K. W. Wong, D. L. Ma, *Angew. Chem., Int. Ed.* **2018**, *57*, 13349.
[23] A. Dorcier, W. H. Ang, S. Bolano, L. Gonsalvi, L. Juillerat-Jeannerat, G. Laurenczy, M. Peruzzini, A. D. Phillips, F. Zanobini, P. J. Dyson, *Organometallics* **2006**, *25*, 4090–4096.
[24] J. J. Soldevila-Barreda, P. J. Sadler, *Curr. Opin. Chem. Biol.* **2015**, *25*, 172–183.
[25] A. Marrone, R. H. Fish, *Organometallics* **2023**, *42*, 288–306.
[26] W. Y. Zhang, H. E. Bridgewater, S. Banerjee, J. J. Soldevila-Barreda, G. J. Clarkson, H. Shi, C. Imberti, P. J. Sadler, *Eur. J. Inorg. Chem.* **2020**, 1052–1060.
[27] M. M. Milutinović, J. V. Bogojeski, O. Klisurić, A. Scheurer, S. K. Elmroth, Ž. D. Bugarčić, *Dalton Trans.* **2016**, *45*, 15481–15491.
[28] J. J. Soldevila-Barreda, A. Habtemariam, I. Romero-Canelón, P. J. Sadler, *J. Inorg. Biochem.* **2015**, *153*, 322–333.
[29] M. Shivakumar, J. Gangopadhyay, A. Chakravorty, *Polyhedron* **2001**, *20*, 2089–2093.
[30] S. Banerjee, J. J. Soldevila-Barreda, J. A. Wolny, C. A. Wootton, A. Habtemariam, I. Romero-Canelón, F. Chen, G. J. Clarkson, I. Prokes, L. Song, P. B. O'Connor, V. Schünemann, P. J. Sadler, *Chem. Sci.* **2018**, *9*, 3177–3185.
[31] A. Sink, S. Banerjee, J. A. Wolny, C. Imberti, E. C. Lant, M. Walker, V. Schünemann, P. J. Sadler, *Dalton Trans.* **2022**, *51*, 16070–16081.
[32] W. Y. Zhang, S. Banerjee, G. M. Hughes, H. E. Bridgewater, J. I. Song, B. G. Breeze, G. J. Clarkson, J. P. Coverdale, C. Sanchez-Cano, F. Ponte, E. Sicilia, P. J. Sadler, *Chem. Sci.* **2020**, *11*, 5466–5480.
[33] R. A. Krause, K. Krause, *Inorg. Chem.* **1984**, *23*, 2195–2198.

[34] S. Patai, *The Chemistry of the Hydrazo, Azo and Azoxy Groups* Vol. *1*, Wiley, Hoboken **2010**.
[35] S. J. Dougan, A. Habtemariam, S. E. McHale, S. Parsons, P. J. Sadler, *Proc. Natl. Acad. Sci. U S A.* **2008**, *105*, 11628–11633.
[36] Y. Fu, *Ph.D Thesis*, University of Warwick (Warwick) **2011**.
[37] H. Schlundt, *J. Phys. Chem.* **2002**, *5*, 503–26.
[38] D. L. Nelson, M. M. Cox, *Lehninger Principles of Biochemistry*, W. H. Freeman, New York **2017**.
[39] V. Vichai, K. Kirtikara, *Nat. Protocl.* **2006**, *1*, 1112–1116.
[40] L. Guo, X. Hu, Y. Yang, W. An, J. Gao, Q. Liu, Z. Liu, *Bioorg. Chem.* **2021**, *116*, 105311.
[41] P. Vandenabeele, L. Galluzzi, T. Vanden Berghe, G. Kroemer, *Nat. Rev. Mol. Cell Biol.* **2010**, *11*, 700–714
[42] O. Kepp, L. Galluzzi, M. Lipinski, J. Yuan, G. Kroemer, *Nat. Rev. Drug Discovery* **2011**, *10*, 221–237.
[43] J. P. Coverdale, H. E. Bridgewater, J. I. Song, N. A. Smith, N. P. Barry, I. Bagley, P. J. Sadler, I. Romero-Canelon, *J. Med. Chem.* **2018**, *61*, 9246–55.
[44] T.-Y. Choi, T.-I. C., Y.-R. Lee, S.-K., S.-K. Choe, C.-H. Kim, *Exp. Mol. Med.* **2021**, *53*, 310–317.
[45] E. E. Patton, L. I. Zon, D. M. Langenau, *Nat. Rev. Drug Discovery* **2021**, *20*, 611–628.
[46] A. Rissone, A. F. Candotti, *Bio. Protoc. 2016*, *6*, e1941–e1941.
[47] J. Checa, J. M. Aran, *J. Inflamm. Res.* **2020**, 1057–1073.
[48] R. L. Auten, J. M. Davis, *Pediatr. Res.* **2009**, *66*, 121–127.
[49] M. Schieber, N. S. Chandel, *Curr. Biol.* **2014**, *24*, R453-R462.
[50] N. Xie, L. Zhang, W. Gao, C. Huang, P. E. Huber, X. Zhou, C. Li, G. Shen, B. Zou, *Signal Transduct. Target Ther.* **2020**, *5*, 227.
[51] J. J. Soldevila-Barreda, A. Habtemariam, I. Romero-Canelón, P. J. Sadler, *J. Inorg. Biochem.* **2015**, *153*, 322–333.
[52] D. A. Averill-Bates, in *Vitamins and Hormones* (Ed: G. Litwack), Vol. *121*, Elsevier, Amsterdam **2023**, pp. 109–141.
[53] M. F. Renschler, *Eur. J. Cancer* **2004**, *40*, 1934–1940.
[54] A. F. Peacock, A. Habtemariam, R. Fernández, V. Walland, F. P. Fabbiani, S. Parsons, R. E. Aird, D. I. Jodrell, P. J. Sadler, *J. Am. Chem. Soc.* **2006**, *128*, 1739–1748.
[55] R. J. Needham, C. Sanchez-Cano, X. Zhang, I. Romero-Canelón, A. Habtemariam, M. S. Cooper, L. Meszaros, G. J. Clarkson, P. J. Blower, P. J. Sadler, *Angew. Chem., Int. Ed.* **2017**, *56*, 1017–1020.
[56] S. Goswami, A. R. Chakravarty, A. Chakravorty, *Inorg. Chem.* **1983**, *22*, 602–609.
[57] S. Goswami, R. Mukherjee, A. Chakravorty, *Inorg. Chem.* **1983**, *22*, 2825–2832.
[58] W. G. Kirlin, J. Cai, S. A. Thompson, D. Diaz, T. J. Kavanagh, D. P. Jones, *FreeRadic. Biol. Med.* **1999**, *27*, 1208–1218.
[59] F. Q. Schafer, G. R. Buettner, *FreeRadic. Biol. Med.* **2001**, *30*, 1191–1212.

Manuscript received: November 10, 2024
Revised manuscript received: March 17, 2025
Accepted manuscript online: March 20, 2025
Version of record online: May 7, 2025